Journal of Applied Physics

RESEARCH ARTICLE | OCTOBER 10 2023

Porous pseudo-substrates for InGaN quantum well growth: Morphology, structure, and strain relaxation

Yihong Ji ; Martin Frentrup ; Xiaotian Zhang ; Jakub Pongrácz ; Simon M. Fairclough ; Yingjun Liu ; Tongtong Zhu ; Rachel A. Oliver

J. Appl. Phys. 134, 145102 (2023)
https://doi.org/10.1063/5.0165066

CrossMark

21 February 2024 06:20:27

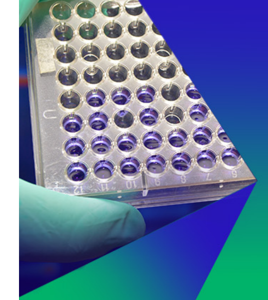

Biomicrofluidics
Special Topic:
Microfluidics and Nanofluidics in India
Submit Today
AIP Publishing

Journal of Applied Physics ARTICLE pubs.aip.org/aip/jap

Porous pseudo-substrates for InGaN quantum well growth: Morphology, structure, and strain relaxation

Cite as: J. Appl. Phys. **134**, 145102 (2023); doi: 10.1063/5.0165066
Submitted: 26 June 2023 · Accepted: 23 September 2023 ·
Published Online: 10 October 2023

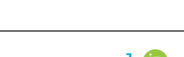

Yihong Ji,[1,a)] Martin Frentrup,[1] Xiaotian Zhang,[1] Jakub Pongrácz,[1,2,3] Simon M. Fairclough,[1] Yingjun Liu,[4] Tongtong Zhu,[4] and Rachel A. Oliver[1,4]

AFFILIATIONS

[1]Department of Materials Science and Metallurgy, University of Cambridge, Cambridge, United Kingdom
[2]Institute of Physics of Materials, Czech Academy of Science, Brno, Czech Republic
[3]Central European Institute of Technology, Brno University of Technology, Brno, Czech Republic
[4]Poro Technologies Ltd, Sawston, Cambridge, United Kingdom

[a)]**Author to whom correspondence should be addressed:** yj335@cam.ac.uk

21 February 2024 06:20:27

ABSTRACT

Strain-related piezoelectric polarization is detrimental to the radiative recombination efficiency for InGaN-based long wavelength micro-LEDs. In this paper, partial strain relaxation of InGaN multiple quantum wells (MQWs) on the wafer scale has been demonstrated by adopting a partially relaxed InGaN superlattice (SL) as the pseudo-substrate. Such a pseudo-substrate was obtained through an electro-chemical etching method, in which a sub-surface InGaN/InGaN superlattice was etched via threading dislocations acting as etching channels. The degree of strain relaxation in MQWs was studied by x-ray reciprocal space mapping, which shows an increase of the in-plane lattice constant with the increase of etching voltage used in fabricating the pseudo-substrate. The reduced strain in the InGaN SL pseudo-substrate was demonstrated to be transferable to InGaN MQWs grown on top of it, and the engineering of the degree of strain relaxation via porosification was achieved. The highest relaxation degree of 44.7% was achieved in the sample with the porous InGaN SL template etched under the highest etching voltage. Morphological and structural properties of partially relaxed InGaN MQWs samples were investigated with the combination of atomic force and transmission electron microscopy. The increased porosity of the InGaN SL template and the newly formed small V-pits during QW growth are suggested as possible origins for the increased strain relaxation of InGaN MQWs.

© 2023 Author(s). All article content, except where otherwise noted, is licensed under a Creative Commons Attribution (CC BY) license (http://creativecommons.org/licenses/by/4.0/). https://doi.org/10.1063/5.0165066

I. INTRODUCTION

Micro-displays require the development of highly efficient green, amber, and red light-emitting diodes (LEDs) to a few micrometer size, but significant challenges remain in the development of InGaN-based micro-LEDs across the full-color range.[1–4] This necessitates a high In content ($x \geq 0.2$) in $In_xGa_{1-x}N$ for long wavelength emission which leads to a large lattice mismatch between the InGaN and GaN layers of the LED's active region, resulting in a strong piezoelectric field across the multi quantum wells (MQWs) in the active region of the c-plane wurtzite GaN. This piezoelectric field (together with the natural difference in spontaneous polarization) reduces the electron–hole wavefunction overlap in InGaN MQWs. This allows non-radiative recombination processes to compete more successfully with the radiative processes, lowering the radiative recombination efficiency of injected carriers.[5] Furthermore, additional structural defects such as misfit dislocations and stacking faults,[6,7] sometimes accompanied by V-pits[8] and trench defects,[9] tend to form during the overgrowth of the epilayer due to the large lattice mismatch. Moreover, compressive stress stored in InGaN layers reduces the In incorporation efficiency during epitaxial growth of the LED heterostructure, known as the compositional pulling effect.[10] This limits the range of achievable emission wavelengths and, hence, further hinders the application of InGaN micro-LED devices in the long wavelength regime.[11]

© Author(s) 2023

The detrimental strain-related polarization and pulling effects could be potentially relieved by adopting a porous structure within the nitrides. This porous nitride structure contains a large density of small holes or pores, typically formed inside highly doped GaN or InGaN layers. Porous nitrides have a lower stiffness compared to non-porous layers and, hence, are more compliant and able to adopt the larger in-plane lattice constants of the subsequently overgrown high In content InGaN layers of the LED active region.[12] In several reports, the group of Mishra has demonstrated an increased strain relaxation and a potentially higher In incorporation efficiency in InGaN layers grown on pre-patterned micrometer-size porosified GaN pseudo-substrates, where the porosification of the heavily doped regions of GaN was achieved by electro-chemical etching (ECE) via mesa sidewalls.[13–15] However, fabricating such pseudo-substrates involves multiple processing steps, such as patterning and dry etching, and the patterned structures are limited in size, which may make this method very costly and unattractive to implement.

Here, we make use of an alternative strategy to porosify InGaN-based superlattice (SL) heterostructures on the wafer scale via ECE through dislocation pipes, where dislocations across the heterostructure serve as a vertical channel to access the sub-surface doped III-nitride layers to the etching acid. Porosification is achieved by etching the n-doped layers and transporting the dissolved material out of the structure through the dislocation pipes, leaving pores in the etched nitride layer.[16] Although there is limited evidence as to which type of dislocations act as the predominant etching channels, such data available, suggests that all types of threading dislocations (edged, mixed, and screw) can act as such channels.[17] This technique can be easily applied at the wafer scale—theoretically of any wafer size (here, we use a 2-in. wafer)—and does not require any additional lithographic processing steps. The structural and morphological properties of such porous heterostructures have been analyzed for suitability to serve as partially relaxed pseudo-substrates. Following that, a set of InGaN MQWs has been grown on pre-porosified InGaN SL pseudo-substrates, etched under different voltages, to investigate the impact of etching voltage on the degree of strain relaxation and how the properties of the template transfer to MQWs.

II. SAMPLE DETAILS AND METHODS

Two types of samples were investigated in this study: a set of two InGaN SL templates (A) and a set of InGaN MQWs samples grown on top of such InGaN SL templates (B). All samples used in this study were provided by Poro Technologies Ltd (Porotech) and were grown on 2-in. sapphire substrates. Figure 1(a) shows a schematic structure of the as-grown SL template (sample A1); the substrate consists of a 2 μm-thick GaN buffer layer, followed by 250 nm of undoped GaN (un-GaN). Ten pairs of 20 nm-thick unintentionally doped $In_{0.11}Ga_{0.89}N$ (un-InGaN) and highly n-doped $In_{0.07}Ga_{0.93}N$ (n-InGaN) layers were grown on top of it. The n-dopant was Si, and the nominal doping density in the n-doped layers was 1×10^{19} cm^{-3}. This superlattice was capped by 20 nm of undoped $In_{0.12}Ga_{0.88}N$.

The porosification of the InGaN SL templates was achieved via a simple one-step ECE process at room temperature without UV illumination, using 0.25 M oxalic acid as the electrolyte and a constant DC voltage of 6 V and above, between the n-doped GaN layers (anode) and an inert platinum foil as the counter electrode (cathode).[17] The sub-surface etching that penetrated through the undoped cap was intended to occur via etching channels that form along the core of threading dislocations across the heterostructure, similar to the porosification of GaN as described in detail in Ref. 16. The etching process was controlled by monitoring and recording the etch current signal with a Keithley 2400 source meter. After etching, the samples were rinsed with de-ionized water and blow-dried in N_2.[17] The schematic structure of the porosified SL template (sample A2) is illustrated in Fig. 1(b).

For the second set of samples illustrated in Fig. 1(c), InGaN MQWs consisting of five pairs of approximately 7 nm $In_{0.06}Ga_{0.94}N$ quantum barriers (QBs) and 3 nm $In_{0.1}Ga_{0.9}N$ QWs were grown on three different porosified InGaN SL templates. These three templates were etched under different voltages to achieve different porosities across the templates and, thus, to engineer the stiffness of the templates. This allows us to study the impact of porosification on the strain relaxation of InGaN MQWs. These three samples are classified as the least-etched sample (sample B1), medium-etched sample (sample B2), and the most-etched sample (sample B3), accordingly.

21 February 2024 06:20:27

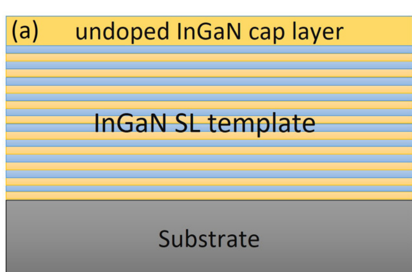

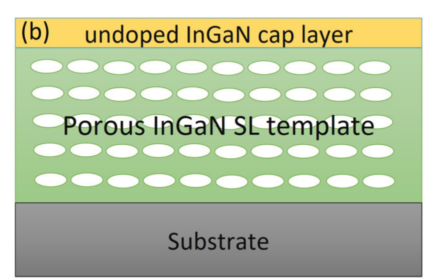

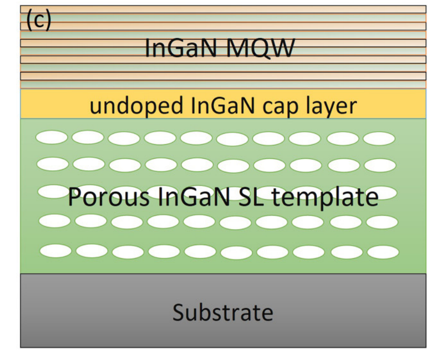

FIG. 1. Schematic structure illustration of (a) as-grown InGaN SL templates, (b) porosified InGaN SL templates, and (c) InGaN MQWs grown on a porosified SL template.

© Author(s) 2023

To facilitate the analysis, each MQW sample of this second sample set (B set) was divided into two regions; the porosified center and the non-porous region at the outer edge of the sample. As will be shown below, a comparison between the porosified region and non-porous region within one sample reveals how porosification affected the morphology, while a comparison of the porosified regions among the three samples will provide information about the influence of etching degree on the surface morphology.

High-resolution x-ray diffraction (XRD) was employed to determine the structural properties of all samples. The in-plane lattice constant and relaxation degree of the heterostructures were determined from reciprocal space maps (RSMs) of four different off-axis reflections, using a PANalytical Empyrean diffractometer equipped with a two-bounce hybrid monochromator and a PIXcel CCD detector operated in a frame-based mode. XRD ω–2θ scans of the 0002 reflection were measured with the PANalytical X'pert diffractometer in triple-axis configuration to determine the layer thickness and alloy composition of both SL template samples A1 and A2. The best match of these two parameters was obtained by matching simulations of the PANalytical Epitaxy software package to the measured XRD intensity data.

The surface morphology of the samples used in this study was measured by atomic force microscopy (AFM) with a Bruker Dimension Icon Pro in the PeakForce tapping mode, using ScanAsyst-Air tips with a nominal tip radius of 2 nm.

To assess the pore morphology of the samples, cross-sectional transmission electron microscopy (TEM) specimen lamellas have been prepared to a thickness of ∼100 nm. All lamellas investigated in this study were prepared with a Field Electron and Ion (FEI) Helios DualBeam Nanolab Focused Ion Beam (FIB) instrument utilizing standard processing techniques and a gallium ion energy of 30 kV (5 kV for the final polish). Scanning transmission electron microscopy-high angle annular dark field (STEM-HAADF) studies were conducted in an FEI Tecnai Osiris TEM, operated at 200 kV, to characterize the cross-sectional structures of all samples used in this study with a beam current of about 40–100 pA and a convergence angle of about 23 mrad.

For the statistical analysis of porosity in the investigated samples, pore morphology seen in the STEM images across 1 μm of specimen for each sample has been analyzed graphically, using the brightness contrast between pores (dark) and remaining InGaN material (bright) areas. This approach provides a lower limit for the average porosity across the full SL of the heterostructures. An example of such an analysis is illustrated in the supplementary material.

III. RESULTS AND DISCUSSION

A. The impact of porosification on InGaN SL templates

Figure 2 shows the cross-sectional STEM-HAADF images of an as-grown InGaN SL template A1 and a porosified InGaN SL template A2. As shown in Fig. 2(a), the bright and dark contrast within the SL corresponds to the u-InGaN and n-InGaN layers, respectively. Threading dislocations (TDs) arising at the GaN/sapphire interface (not shown) extend upward and open to form large V-pits at the surface. Weak beam dark field imaging in TEM suggests that these large V-pits relate predominantly to mixed type (a + c type) dislocations. Figure 2(b) shows the structure of the InGaN SL template after ECE, with alternating porous and

21 February 2024 06:20:27

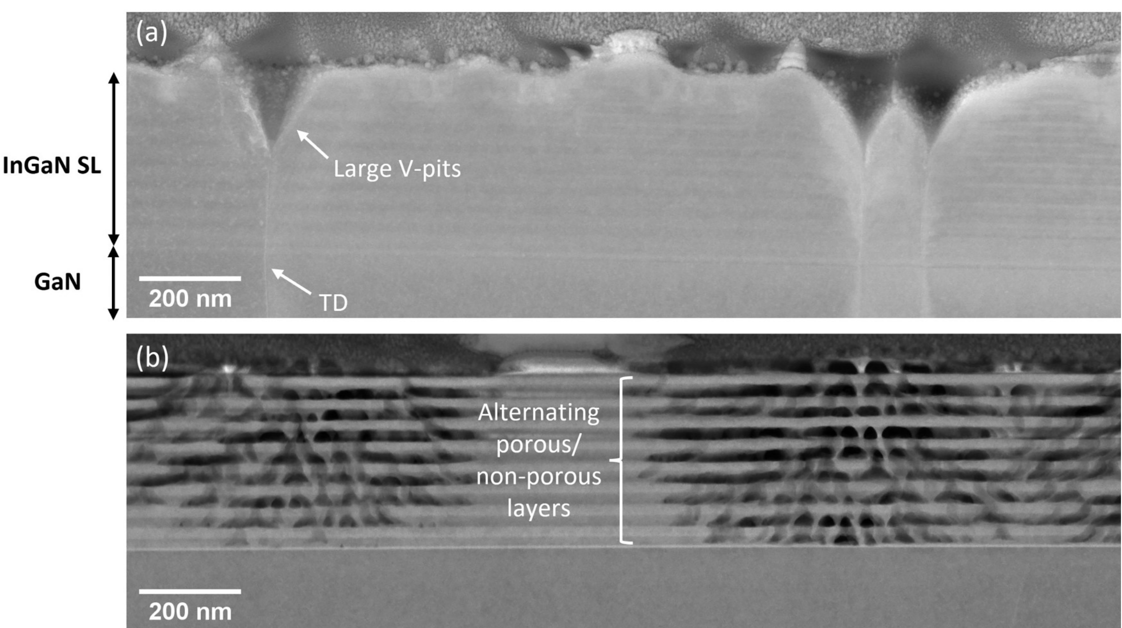

FIG. 2. STEM-HAADF images of the (a) as-grown InGaN SL template A1 and the (b) porosified InGaN SL template A2.

© Author(s) 2023

non-porous layers. It is worth noting that though the V-pits form a short-cut etching route to the first few sub-surface layers, they do not penetrate through the whole stack of the InGaN SL; so the formation of nanopipes at dislocation cores will still be required for the etchant to access lower layers in the stack. The porosification of the sub-surface SL structure was achieved by removing ionized Ga and In out of the highly n-doped $In_{0.07}Ga_{0.93}N$ layers and leaving pores behind, while the unintentionally doped $In_{0.11}Ga_{0.89}N$ layers remained intact. The pores are not homogenously distributed among the porosified layers and radiate from TDs into the adjoining doped layers. It should be noted that porosification via dislocation-related channels has been observed in structures such as GaN-distributed Bragg reflectors to achieve a much higher homogeneity than is observed here, suggesting that homogeneity is dependent on both the epitaxial structure and the etching conditions.[16]

To investigate the influence of porosification of InGaN SL template structures seen in the previous STEM images on the strain relaxation properties, RSMs of the GaN $10\bar{1}4$ reflection shown in Fig. 3 were recorded to extract the in-plane lattice parameters for both samples. As can be seen in Fig. 3(a), the as-grown InGaN SL is fully strained to the GaN substrate, as the diffraction peaks are well aligned with each other at (nearly) the same Q_x coordinate. For the porosified InGaN SL template A2 [Fig. 3(b)], on the other hand, the InGaN SL peak shifts toward the smaller $|Q_x|$ side, indicating a larger in-plane lattice constant and that partial strain relaxation has been achieved in the InGaN SL. For strain analysis, the in-plane lattice constant of the porosified SL was obtained from the four RSMs of the $10\bar{1}4$, $10\bar{1}5$, $20\bar{2}4$, and $20\bar{2}5$ reflections, which gives the value of the in-plane lattice constant (3.1974 ± 0.0002) Å [equivalent to fully relaxed $In_xGa_{1-x}N$ with a composition of $x = (0.0224 \pm 0.0006)$].

Figure 4 shows high-resolution ω–2θ scans of the 0002 reflection, which have been collected to determine the average SL period thickness and alloy composition. Assuming that the SL is fully strained to the GaN buffer in the as-grown reference sample (as evidenced by the RSMs), the best-matched simulation reveals that the $In_xGa_{1-x}N$ reference SL structure consists of ten periods of (19.00 ± 0.05) nm, $x = (9.15 \pm 0.05)\%$ un-$In_xGa_{1-x}N$ and (19.00 ± 0.05) nm, $x = (6.10 \pm 0.05)\%$ n-$In_xGa_{1-x}N$.

Compared to the as-grown SL sample A1 [the black solid line in Fig. 4(a)], the satellite peaks of porosified SL A2 (red dashed line) have shifted to the larger diffraction angles, while their separation remains nearly the same. To account for the partial relaxation of the porosified SL sample, the heterostructure was simulated with a fully relaxed infinitesimally thin layer inserted between the InGaN SL and the GaN buffer layer. This infinitesimally thin layer was assumed to have a composition of $x = 0.0224\%$ to match the in-plane lattice constant of the InGaN SL previously determined from the reciprocal space maps, and the simulated InGaN SL was assumed to match this thin layer at the interface. The simulation revealed that most of the peak shift observed in the ω–2θ scan is caused by the partial strain relaxation of the porosified InGaN SL. An additional small shift is caused by a small compositional variation between both samples. The best match of the simulation with the measured data gives for the structure of the porosified InGaN SL: ten periods of (19.00 ± 0.05) nm, $x = (8.85 \pm 0.05)\%$ un-$In_xGa_{1-x}N$/ (19.00 ± 0.05) nm, and $x = (5.90 \pm 0.05)\%$ n-$In_xGa_{1-x}N$. The corresponding degree of strain relaxation was calculated as 24.9%. A

21 February 2024 06:20:27

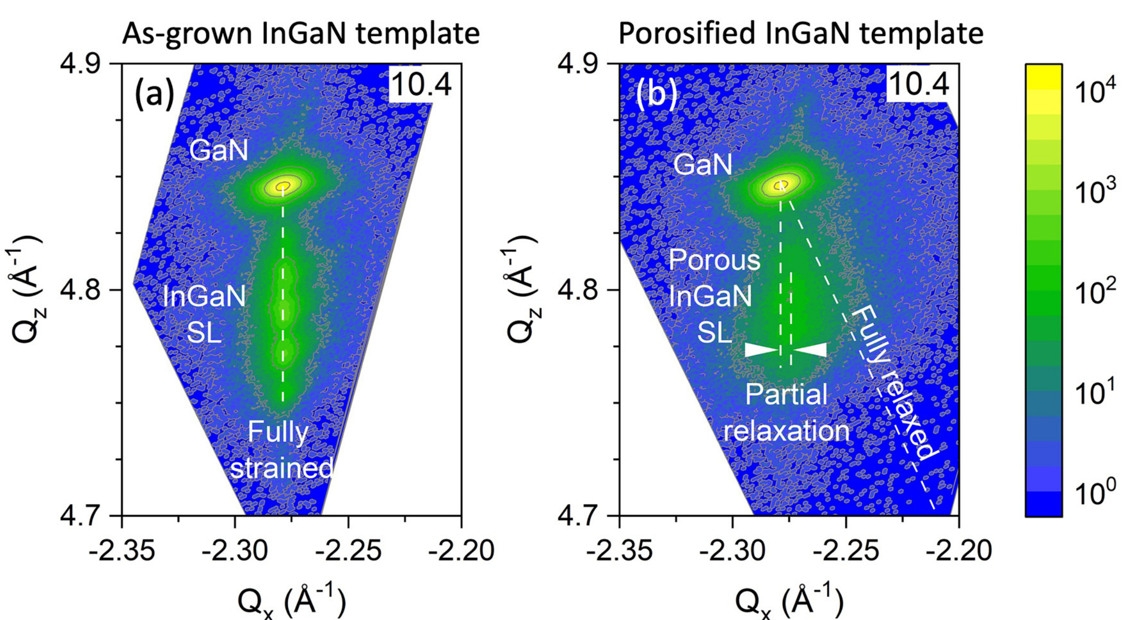

FIG. 3. RSMs from GaN $10\bar{1}4$ reflection for (a) the as-grown InGaN SL template A1 and (b) the porosified InGaN SL template A2.

© Author(s) 2023

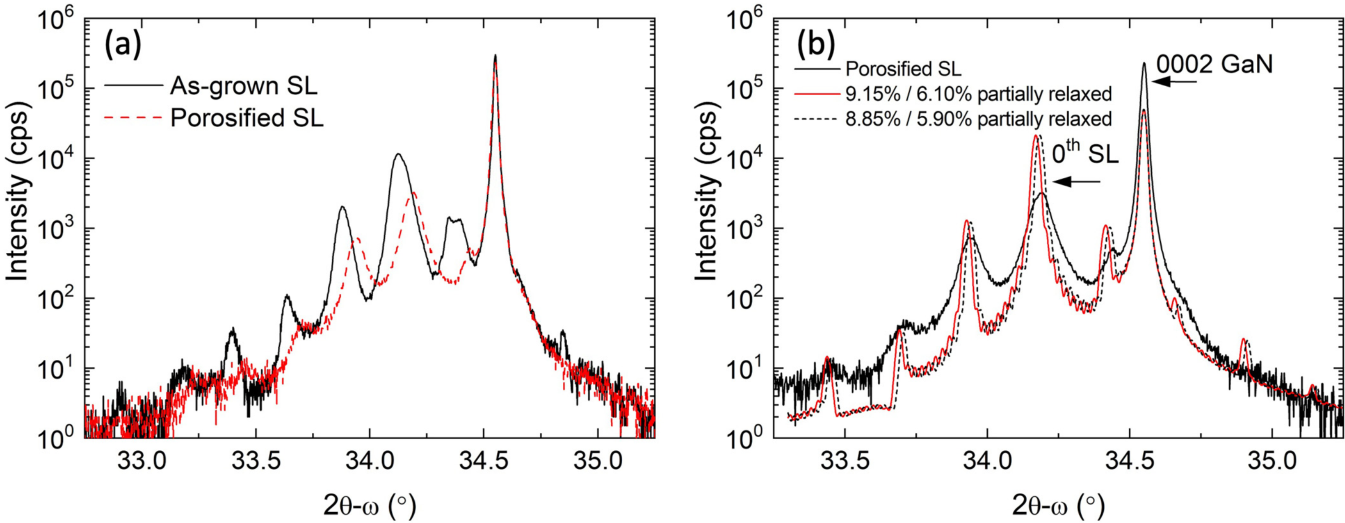

FIG. 4. (a) Measured $\omega - 2\theta$ scans of the 0002 reflection of porosified and as-grown SL. (b) Measured ω–2θ scan and simulation of a porosified SL.

further relaxation may be achievable via optimization of porosification, which we will discuss more in detail later in Sec. II.

As seen in the HAADF STEM image, the pores seen in the porosified InGaN SL template [Fig. 2(b)], which provide free space for elastic strain relaxation, may partly account for the partial strain relaxation we observed from RSMs. Other possible sources of strain relaxation could be changes in elastic strain relaxation via changes in surface roughness. Here, it is interesting to look at surface V-pits, since an increase in the size of V-pits formed during epitaxy could lead to an increase in relaxation, and the generation of new surface V-pits could indicate the formation of new threading dislocations associated with dislocation loops inside the InGaN SL layers, including misfit dislocation segments. AFM was performed to investigate the surface morphology, to address these possibilities.

Representative AFM scans for both the as-grown and the porosified InGaN SL templates are shown in Figs. 5(a) and 5(b), respectively. Typical surface defects such as large V-pits and trench defects are present in both samples, whereas occasional small V-pits can only be observed on the surface of the porosified template. The surface between those pits appears to consist of steps and terraces in both samples with similar root mean square (rms)-roughness (of roughly 0.4 nm in those pit-free regions). A statistical analysis of large V-pits from $10 \times 10\,\mu m^2$ AFM scans across five different areas that are several 100 s of micrometers apart from each sample suggests only a small variation in depth (35 ± 14) nm within the error margin, while their density and distribution remain the same $[(3.0 \pm 0.2) \times 10^8\,cm^2]$. (These depths are consistent with the depths of large V-pits shown in Fig. 2, bearing in mind that the AFM tip will not penetrate all the way to the bottom of the observed structures.) This small size variation of large V-pits is reasonable because the large V-pits open up at the apex of threading dislocations that originate from the GaN/sapphire interface during growth, and hence, their presence should not be affected by porosification.

The slight increase in size observed is not sufficient to cause strain relaxation in the porosified SL template shown by the XRD data. However, the presence of small V-pits in the porosified SL template is a new surface feature compared with the non-porous SL template. These small V-pits might be related to edge-type threading dislocations, which do not open up into V-pits during growth, but may open up during ECE.[18]

The results have shown so far that the porosification of the highly n-doped InGaN layers (see Fig. 2), which may help to reduce the stiffness of the SL structure, combined with the small V-pits could explain the observed strain relaxation in the porosified SL template.

B. The impact of porosification of the SL on the overgrown MQWs

In the previous section (Sec. I), we have shown that porosification can lead to a partial relaxation of the InGaN SL template. In this section, we will investigate how different degrees of porosity in the InGaN SL templates influence the morphological and structural properties of MQWs grown on such porous templates. For this purpose, three different MQW samples overgrown on porous templates were investigated. The porous templates differed in voltages applied during the electro-chemical etching of the template. Non-porous regions of each sample were also investigated as controls.

Figure 6 shows the cross-sectional STEM-HAADF images of MQWs grown on top of the (a) non-porosified reference region of sample B2, and on top of the InGaN SL templates, previously porosified at (b) low (sample B1), (c) medium (sample B2), and (d) high (sample B3) voltages. At the bottom of each image, the GaN

21 February 2024 06:20:27

© Author(s) 2023

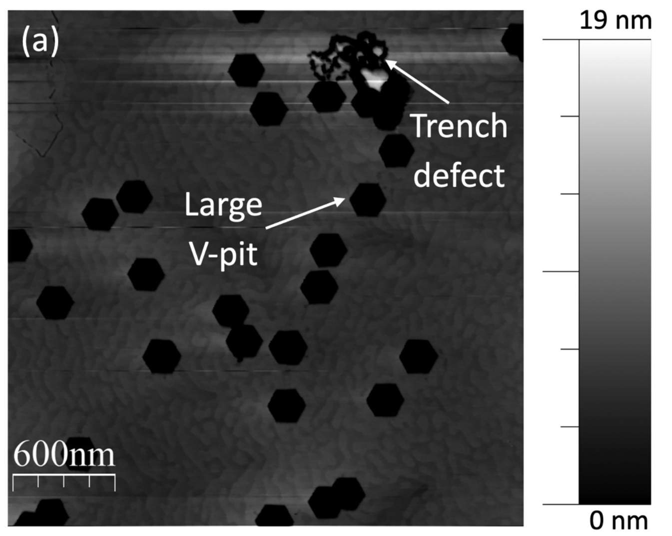

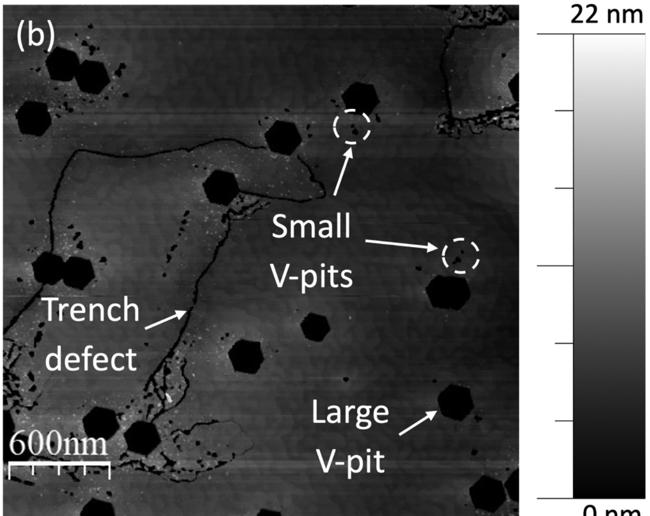

FIG. 5. InGaN SL template surface morphologies comparison between (a) as-grown InGaN SL A1 and (b) porosified InGaN SL A2. Scan size is $3 \times 3\,\mu m^2$.

buffer layer is visible, followed by the InGaN SL template with its alternating layers of slightly different compositions and a final cap layer. On top of this, InGaN QWs and barriers are visible as very thin layers with different brightness contrast. In Fig. 6(a), large V-pits penetrate the InGaN SL template, which are related to threading dislocations originating from the sapphire substrate, whereas small V-pits are confined within InGaN MQWs.

1. Variations in the pore structure

Below, we will initially focus our discussion on the variation in the pore structure and will come back to the distribution of small V-pits at a later point in this section.

In the etched templates, the pore structure of the porosified SL changed dramatically with the etching voltage used for the porosification of the template. For the lowest etched sample B1 in

21 February 2024 06:20:27

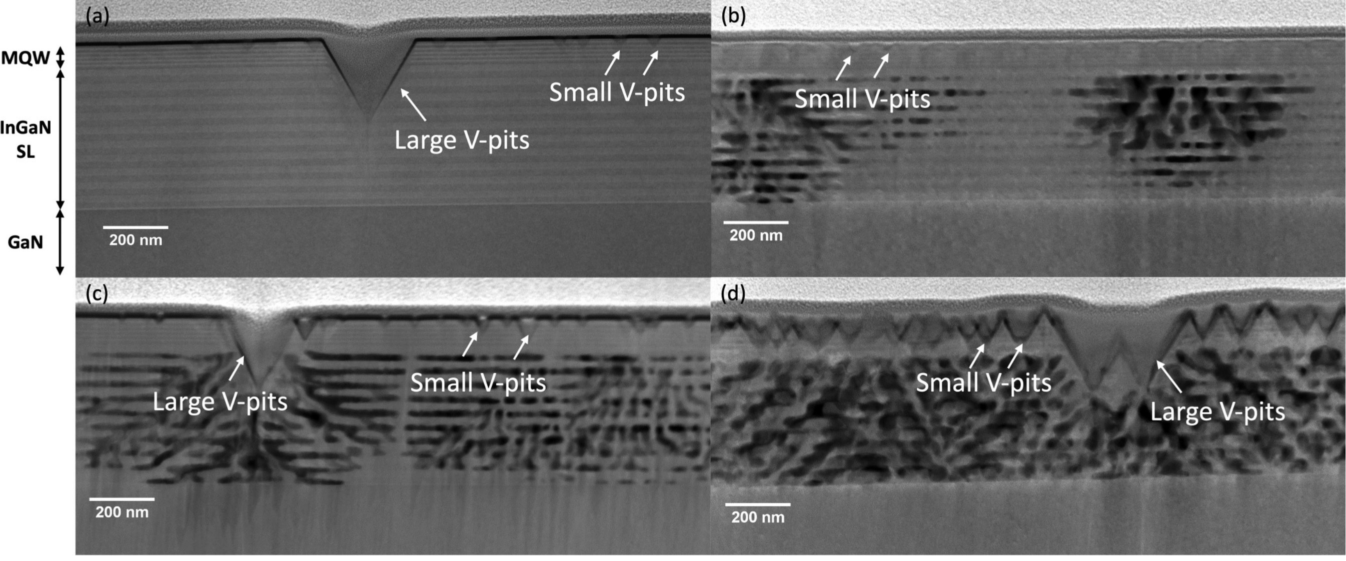

FIG. 6. Cross-sectional STEM-HAADF images of (a) the non-porous region of sample B2 and (b) the porosified regions of sample B1, (c) sample B2, and (d) sample B3.

© Author(s) 2023

Fig. 6(b), discrete patches of pores can be observed in the highly n-doped InGaN layers. Where porosity is present, the porosified SL maintains a structure of alternating porous/non-porous layers, which correspond to the highly n-doped/undoped layers. For the medium-etched sample B2 in Fig. 6(c), a much more uniform porosification is observed with only narrow non-porous regions. The pores in the doped InGaN SL layers increase in size. Most of them extend laterally along the n-doped InGaN SL layers. Close to large V-pits, it appears that pores spread out normal to the facets of the V-pits, which could be related to the local electric field distribution.[12] In the most-etched sample, as shown in Fig. 6(d), the n-doped layers in the SL are completely porosified and pores from different layers coalesce so that the alternating porous and non-porous InGaN layers of the SL are no longer clearly distinguishable. Figure 6 quantifies the trend observed in the images: the porosity of the SL as a whole increases monotonically with the increasing etching voltage and reaches its maximum at about (45 ± 1.3)% for the most-etched InGaN template B3.

2. Influence of porosity on strain relaxation

To investigate how the variation in porosity influences the in-plane strain and relaxation of the template and the overgrown MQWs, XRD reciprocal space maps of the $10\bar{1}4$, $10\bar{1}5$, $20\bar{2}4$, and $20\bar{2}5$ off-axis reflections have been collected for each sample. Figures 7(a) and 7(b) show the representative RSMs of the $10\bar{1}4$ reflection for the non-porous and porosified regions of the medium-etched sample B2, respectively. In case of the non-porous region, the clearly visible satellite peaks of the SL template and MQWs below the GaN peak superimpose each other. (However, they can be clearly identified from the very different periodicity/layer thicknesses of both superlattices.) The vertical dashed lines show that they all share approximately the same in-plane coordinate Q_x, which means that the InGaN SL and MQWs are fully strained to GaN. For the porosified region, the periodic fringes from the InGaN SL and MQWs are significantly weaker due to diffuse scattering from pore walls in the InGaN template. However, a clear Q_x-shift of the peak positions can be observed revealing that the InGaN SL partially relaxed as a result of porosification, and that this relaxation is passed to the overgrown MQWs. An analysis of the peak positions from four different RSMs for the porosified regions reveals a systematic increase in the in-plane lattice parameter (3.1962 ± 0.0010), (3.2012 ± 0.0010), and (3.2026 ± 0.0010) Å with increasing porosity (samples B1, B2, and B3). In theory, these lattice parameters are equivalent to the values of fully relaxed InGaN with an In content of x = (1.91 ± 0.28)%, x = (3.32 ± 0.28)%, and (3.72 ± 0.28)%, respectively. The largest in-plain lattice parameter of 3.2026 Å reported here is comparable to that obtained by other wafer-scale technologies, such as InGaNOS,[11] for the fabrication of relaxed InGaN pseudo-substrates. In-plane lattice parameters of up to 3.2069 Å have been reported in the case of InGaNOS-based templates from Soitec™.[19]

The information on the in-plane lattice constant was used for simulations of ω–2θ-scans, using the same approach as in Sec. I for the InGaN SL templates without MQWs. These measurements (not shown) reveal that the periodicity across the samples varies slightly and that the average composition of each period in the SL increased as the volume amount of the doped layers containing low-In content reduced due to etching.

So far, experimental results have shown that an increase in the etching voltage during the porosification process increases the average porosity in the SL templates, whereas the strain in the SL template and MQWs reduces, although even the most relaxed samples are only partially relaxed. Now, we turn our attention toward the surface morphology of these samples.

3. Surface morphology

The STEM-HAADF characterization of MQWs given in the top part of Figs. 6(a)–6(d) shows large differences in the density of small V-pits. In the non-porous reference region Fig. 6(a) and the least-etched sample Fig. 6(b), the surface appears relatively smooth with a few very small V-pits separated from each other by distances >100 nm penetrating into the uppermost (and in rare cases, into

21 February 2024 06:20:27

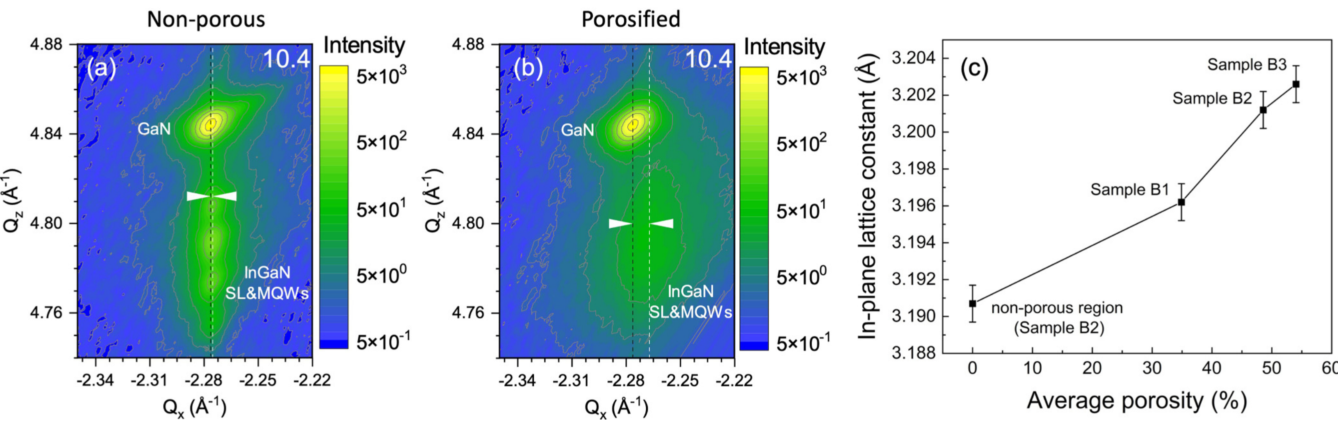

FIG. 7. XRD RSMs of the (a) non- porous region and (b) porous region of sample B2. (c) In-plane lattice constant as a function of the average porosity.

© Author(s) 2023

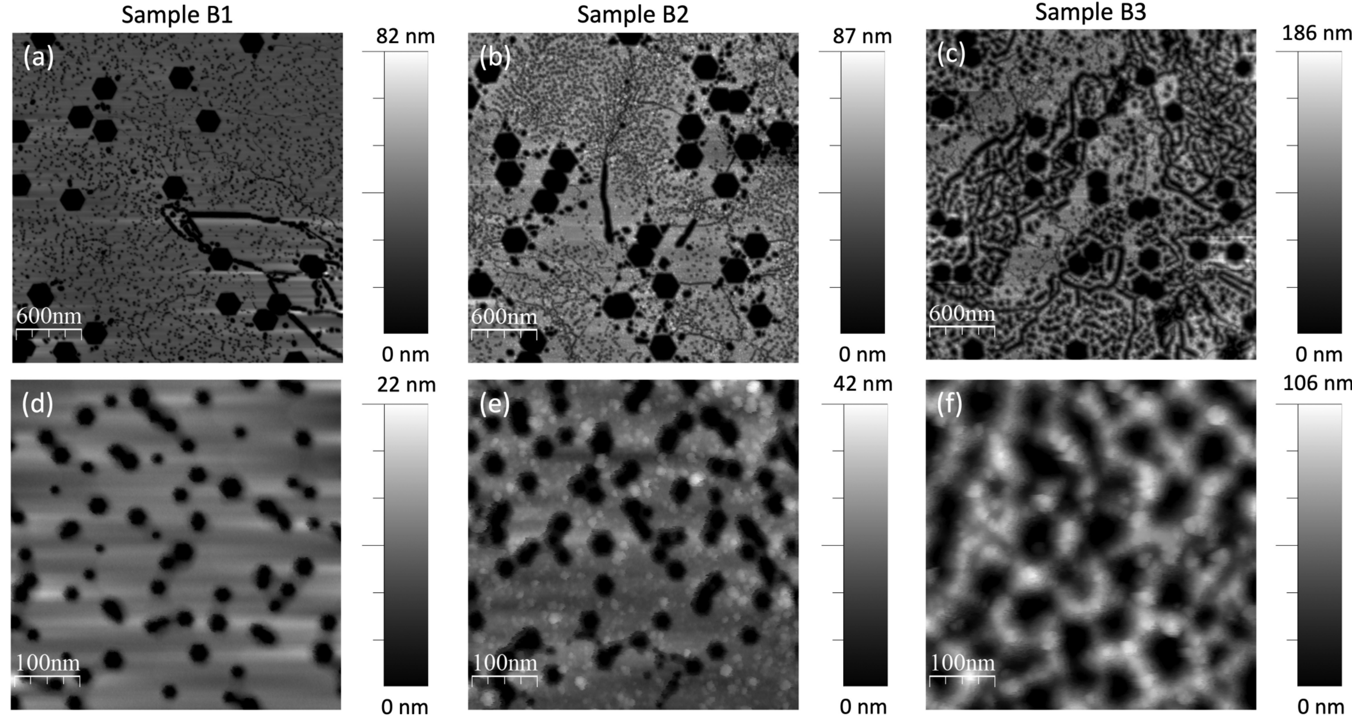

FIG. 8. AFM scans provide an overview of the surface morphologies of InGaN MQWs grown on the porosified regions of samples B1, B2, and B3 [(a)–(c)]. Magnified images of the regions between large V-pits, where only small V-pits are present [(d)–(f)].

21 February 2024 06:20:27

one additional) QW in the MQW stack. In the medium-etched sample, Fig. 6(c), the average spacing between small V-pits on the surface reduces to only a few 10 s of nm and some of the small V-pits appear larger in size and penetrate into the top 2nd and 3rd QW. In the most-etched sample, porosified at the highest voltage, the quantity (and size) of small V-pits increased so much that they disrupted the continuity of QWs completely and left a very rough surface behind.

This increased small pit concentration was also confirmed by AFM measurements of the sample surface of the three MQW samples, as shown in Fig. 8. In the $3 \times 3\,\mu m^2$ overview scans (top row), three pronounced surface features, i.e., large V-pits, small V-pits, and trench defects, are present on all samples. Among them, large V-pits are distributed evenly across the scanned regions for all samples, and there is no obvious difference with regard to the size and density ($\sim 3 \times 10^8\,cm^2$) and distribution of large V-pits for these three samples. Considering large V-pits were observed on the porosified SL template before the overgrowth of InGaN MQWs, this may indicate that the large V-pits were not affected either by the overgrowth or the increased etching voltage, which is in agreement with the observations made in Sec. I. However, in Fig. 8, the density of small V-pits increased significantly with the etching voltage from samples B1 to B3. On the surface of the least-etched sample (B1), a few small V-pits are sporadically distributed with a density of about $(2.73 \pm 0.28) \times 10^{10}\,cm^{-2}$ as measured from four different $0.5 \times 0.5\,\mu m^2$ regions across the surface. On the surface of the medium-etched sample (B2), they have slightly increased in number $[(3.81 \pm 0.52) \times 10^{10}\,cm^{-2}]$ and appeared in the periphery of large V-pits. In the most-etched sample (B3), they evenly spread all over the surface and merged with each other, so that it was not possible to determine a meaningful density of V-pits. Note that the provided errors are the standard errors—the standard deviation of the mean divided by the square root of the number of measurements for each sample—hence, the small values of the errors indicate a fairly uniform distribution of small V-pits across each sample.

IV. DISCUSSION

In MQWs grown on partially relaxed InGaN templates, we observe a high density of newly formed small V-pits. Some of these small V-pits might be related to edge-type threading dislocations from the pseudo-substrate, which did not open up into V-pits during superlattice growth but may open up during ECE or QW overgrowth.[18] However, our TEM studies to date, do not provide evidence for this suggestion. Alternatively, these small V-pits could be related to defects newly formed in the InGaN quantum wells. Possible defect structures include dislocation loops and stacking fault-related structures.[20,21] Dislocation loops in the InGaN epitaxial layer contain two threading dislocation segments, opening up to small V-pits, and have a misfit dislocation segment between those threading dislocations, which can cause plastic strain relaxation. In

© Author(s) 2023

trench defects sub-surface stacking faults, with associated stacking misfit boundaries (SMB), where V-pits open up at changes in orientation in the SMB,[22] contributing to strain relaxation. Eventually, such V-pits merge to form a continuous trench, and this defect structure is often referred to as a "trench defect." However, in the early stages of trench formation, closely-spaced, distinct small pits are observed.[22] Furthermore, the opening of such V-pits is considered as a potential mechanism itself to relax strain, elastically.[23] Since all of our suggested mechanisms for the introduction of additional small V-pits would be expected to result in some strain relaxation, it is surprising to see that the highest density of these newly formed V-pits is observed in MQWs grown on the most relaxed InGaN template. This suggests that other driving forces for the increased formation of these defects need to be considered as well. We intend, in future TEM studies, to investigate which—if any—of the postulated defect structures are connected to the small V-pits, in order to further understand their formation mechanism.

At this point, we may be able to provide a relatively complete picture of the mechanisms behind the increased strain relaxation from samples B1 to B3. As the etching voltage increased, pores in the highly n-doped layers of the SL template started to grow in number and size, leading to the porosified SL structure transition shown in Figs. 6(b)–6(d) and the monotonically increased porosity from samples B1 to B3 shown in the inset figure of Fig. 7(c). This helped to reduce the stiffness of the SL structure and contributed to strain relaxation, which can be confirmed from the gradually increased in-plane lattice constants. Moreover, the formation of surface V-pits may also contribute to the relaxation. The V-pits may directly allow elastic strain relaxation via expansion of the InGaN layers at the V-pit sidewalls. Alternatively or additionally, they may relate to either the termination of threading dislocations linked to the misfit segment in the MQW or to other defects that have been linked to strain relaxation such as trench defects.[24] Finally, it is worth noting here that samples B1 and B2 indicate that it is possible to achieve substantial strain relaxation in the MQW without excess roughening of the QW, and that further optimization of the QW overgrowth conditions may allow for relaxed QWs, which do not exhibit additional defect formation. Indeed, growth on partially relaxed InGaNOS substrates has been optimized to decrease V-pit formation relative to the unrelaxed material.[25]

V. SUMMARY

Porosification of an InGaN SL via sub-surface etching through dislocation pipes was demonstrated and partial strain relaxation of the porosified SL and InGaN MQWs grown on the porosified SL template at a wafer scale was achieved. It was found that porosification has a significant impact on sample surface morphologies, SL template structures, and strain relaxation. The porosity and the number of small V-pits increased with the etching voltage, and many small V-pits were found coalesced in the most-etched sample B3. With the increase of the etching voltage, the shallow surface small V-pits got deeper and eventually penetrated the 1st InGaN QW, which disrupted the continuous and stratiform structure of InGaN MQWs. These small V-pits may be related to the dislocation loops newly formed during the overgrowth of MQWs, but this point requires further investigation. The increased porosity and potentially misfit sections of the dislocation loops related to small V-pits contribute to the highest strain relaxation of ∼45% in the most-etched sample. Further strain relaxation may be achievable via the optimization of porosification. The partial strain relaxation of InGaN MQWs achieved through the porosification of InGaN SL without patterning suggests that strain relaxation in porosified SL is transferable and provides a promising way to relieve strain in the active region at the wafer scale.

SUPPLEMENTARY MATERIAL

The supplementary material describes in detail the procedure used to analyze the porosity, graphically from STEM images of the investigated samples.

ACKNOWLEDGMENTS

We would like to thank Innovate UK for the financial support within the Collaborative Research and Development scheme "*Porous InGaN for Red LEDs (PIRL)*" (Ref. No. 107470) and the EPSRC for support through Cambridge Royce Facilities Grant (No. EP/P024947/1) and Sir Henry Royce Institute—Recurrent Grant No. EP/R00661X/1. This work was also supported by the Royal Academy of Engineering under the Chair in Emerging Technologies program.

AUTHOR DECLARATIONS

Conflict of Interest

Y. Ji, M. Frentrup, X. Zhang, J. Pongrácz, and S. M. Fairclough have no conflicts to disclose. Y. Liu, T. Zhu, and R. A. Oliver have Patent US20230053213A1 pending.

Author Contributions

Yihong Ji: Investigation (equal); Writing – original draft (lead). **Martin Frentrup:** Investigation (equal); Supervision (equal); Writing – review & editing (lead). **Xiaotian Zhang:** Investigation (equal); Writing – review & editing (equal). **Jakub Pongrácz:** Investigation (equal); Writing – review & editing (equal). **Simon M. Fairclough:** Investigation (equal); Writing – review & editing (equal). **Yingjun Liu:** Conceptualization (equal); Funding acquisition (equal). **Tongtong Zhu:** Conceptualization (equal); Funding acquisition (equal); Writing – review & editing (equal). **Rachel A. Oliver:** Conceptualization (equal); Funding acquisition (lead); Investigation (equal); Supervision (equal); Writing – review & editing (lead).

DATA AVAILABILITY

The data that support the findings of this study are openly available in the University of Cambridge repository Apollo at https://doi.org/10.17863/CAM.101738, Ref. 26.

REFERENCES

[1] J. Bai, Y. Cai, P. Feng, P. Fletcher, X. Zhao, C. Zhu, and T. Wang, "A direct epitaxial approach to achieving ultrasmall and ultrabright InGaN micro light-emitting diodes (μLEDs)," ACS Photonics **7**(2), 411–415 (2020).

21 February 2024 06:20:27

© Author(s) 2023

[2]Z. Wang, S. Zhu, X. Shan, Z. Yuan, Z. Qian, X. Lu, Y. Fu, K. Tu, H. Guan, X. Cui, and P. Tian, "Red, green and blue InGaN micro-LEDs for display application: Temperature and current density effects," Opt. Express **30**(20), 36403–36413 (2022).
[3]J. M. Smith, R. Ley, M. S. Wong, Y. H. Baek, J. H. Kang, C. H. Kim, M. J. Gordon, S. Nakamura, J. S. Speck, and S. P. Denbaars, "Comparison of size-dependent characteristics of blue and green InGaN microLEDs down to 1 μ m in diameter," Appl. Phys. Lett. **116**(7), 071102 (2020).
[4]Z. Zhuang, D. Iida, M. Velazquez-Rizo, and K. Ohkawa, "606-nm InGaN amber micro-light-emitting diodes with an on-wafer external quantum efficiency of 0.56%," IEEE Electron Device Lett. **42**(7), 1029–1032 (2021).
[5]T. D. Moustakas and R. Paiella, "Optoelectronic device physics and technology of nitride semiconductors from the UV to the terahertz," Rep. Prog. Phys. **80**(10), 106501 (2017).
[6]H. K. Cho and G. M. Yang, "Generation of misfit dislocations in high indium content InGaN layer grown on GaN," J. Cryst. Growth **243**(1), 124–128 (2002).
[7]H. Wang, D. S. Jiang, U. Jahn, J. J. Zhu, D. G. Zhao, Z. S. Liu, S. M. Zhang, Y. X. Qiu, and H. Yang, "Investigation on the strain relaxation of InGaN layer and its effects on the InGaN structural and optical properties," Physica B **405**(22), 4668–4672 (2010).
[8]I. H. Kim, H. S. Park, Y. J. Park, and T. Kim, "Formation of V-shaped pits in InGaN/GaN multiquantum wells and bulk InGaN films," Appl. Phys. Lett. **73**(12), 1634–1636 (1998).
[9]T. J. O'Hanlon, F. C. P. Massabuau, A. Bao, M. J. Kappers, and R. A. Oliver, "Directly correlated microscopy of trench defects in InGaN quantum wells," Ultramicroscopy **231**, 113255 (2021).
[10]M. C. Johnson, E. D. Bourret-Courchesne, J. Wu, Z. Liliental-Weber, D. N. Zakharov, R. J. Jorgenson, T. B. Ng, D. E. McCready, and J. R. Williams, "Effect of gallium nitride template layer strain on the growth of $In_xGa_{1-x}N$/GaN multiple quantum well light emitting diodes," J. Appl. Phys. **96**(3), 1381–1386 (2004).
[11]A. Even, G. Laval, O. Ledoux, P. Ferret, D. Sotta, E. Guiot, F. Levy, I. C. Robin, and A. Dussaigne, "Enhanced in incorporation in full InGaN heterostructure grown on relaxed InGaN pseudo-substrate," Appl. Phys. Lett. **110**, 262103 (2017).
[12]P. H. Griffin and R. A. Oliver, "Porous nitride semiconductors reviewed," J. Phys. D: Appl. Phys. **53**, 383002 (2020).
[13]S. S. Pasayat, C. Gupta, M. S. Wong, R. Ley, M. J. Gordon, S. P. Denbaars, S. Nakamura, S. Keller, and U. K. Mishra, "Demonstration of ultra-small (<10 μm) 632 nm red InGaN micro-LEDs with useful on-wafer external quantum efficiency (>0.2%) for mini-displays," Appl. Phys. Express **14**, 011004 (2021).
[14]S. S. Pasayat, R. Ley, C. Gupta, M. S. Wong, C. Lynsky, Y. Wang, M. J. Gordon, S. Nakamura, S. P. Denbaars, S. Keller, and U. K. Mishra, "Color-tunable< 10 μ m square InGaN micro-LEDs on compliant GaN-on-porous-GaN pseudo-substrates," Appl. Phys. Lett. **117**, 061105 (2020).
[15]S. S. Pasayat, C. Gupta, D. Acker-James, D. A. Cohen, S. P. Denbaars, S. Nakamura, S. Keller, and U. K. Mishra, "Fabrication of relaxed InGaN pseudo-substrates composed of micron-sized pattern arrays with high fill factors using porous GaN," Semicond. Sci. Technol. **34**, 115020 (2019).
[16]F. C. P. Massabuau, P. H. Griffin, H. P. Springbett, Y. Liu, R. V. Kumar, T. Zhu, and R. A. Oliver, "Dislocations as channels for the fabrication of sub-surface porous GaN by electrochemical etching," APL Mater. **8**, 031115 (2020).
[17]T. Zhu, Y. Liu, T. Ding, W. Y. Fu, J. Jarman, C. X. Ren, R. V. Kumar, and R. A. Oliver, "Wafer-scale fabrication of non-polar mesoporous GaN distributed Bragg reflectors via electrochemical porosification," Sci. Rep. **7**, 45344 (2017).
[18]A. Bojarska-Cieślińska, Ł Marona, J. Smalc-Koziorowska, S. Grzanka, J. Weyher, D. Schiavon, and P. Perlin, "Role of dislocations in nitride laser diodes with different indium content," Sci. Rep. **11**(1), 21 (2021).
[19]A. Dussaigne, F. Barbier, B. Damilano, S. Chenot, A. Grenier, A. M. Papon, B. Samuel, B. Ben Bakir, D. Vaufrey, J. C. Pillet, A. Gasse, O. Ledoux, M. Rozhavskaya, and D. Sotta, "Full InGaN red light emitting diodes," J. Appl. Phys. **128**, 135704 (2020).
[20]N. Sharma, P. Thomas, D. Tricker, and C. Humphreys, "Chemical mapping and formation of V-defects in InGaN multiple quantum wells," Appl. Phys. Lett. **77**(9), 1274–1276 (2000).
[21]J. Smalc-Koziorowska, E. Grzanka, R. Czernecki, D. Schiavon, and M. Leszczyński, "Elimination of trench defects and V-pits from InGaN/GaN structures," Appl. Phys. Lett. **106**, 101905 (2015).
[22]F. C. P. Massabuau, S. L. Sahonta, L. Trinh-Xuan, S. Rhode, T. J. Puchtler, M. J. Kappers, C. J. Humphreys, and R. A. Oliver, "Morphological, structural, and emission characterization of trench defects in InGaN/GaN quantum well structures," Appl. Phys. Lett. **101**, 212107 (2012).
[23]T. L. Song, "Strain relaxation due to V-pit formation in $In_xGa_{1-x}N$/GaN epilayers grown on sapphire," J. Appl. Phys. **98**, 084906 (2005).
[24]G. Kusch, E. J. Comish, K. Loeto, S. Hammersley, M. J. Kappers, P. Dawson, R. A. Oliver, and F. C. P. Massabuau, "Carrier dynamics at trench defects in InGaN/GaN quantum wells revealed by time-resolved cathodoluminescence," Nanoscale **14**(2), 402–409 (2022).
[25]A. Dussaigne, F. Barbier, B. Samuel, A. Even, R. Templier, F. Lévy, O. Ledoux, M. Rozhavskaia, and D. Sotta, "Strongly reduced V pit density on InGaNOS substrate by using InGaN/GaN superlattice," J. Cryst. Growth **533**, 125481 (2020).
[26]Y. Ji, M. Frentrup, X. Zhang, J. Pongrácz, S. M. Fairclough, Y. Liu, T. Zhu, and R. A. Oliver, Research data supporting "Porous pseudo-substrates for InGaN quantum well growth: morphology, structure and strain relaxation," University of Cambridge repository (2023).

21 February 2024 06:20:27

© Author(s) 2023